AMPLITUDO 5(1) (2026)

AMPLITUDO: Journal of Science & Technology Innovation

https://journals.balaipublikasi.id/index.php/amplitudo/index

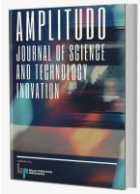

A Comparative Study of Gadobutrol Relaxivity at 3 Tesla for Sustainable Contrast Management and Standardized Phantom Calibration

Maheran Che Ha'[1,2], Izdihar Kamal[2], Mohd Mustafa Awang Kechik[2], Khairil Amir Sayuti[3], Yusri Mohammed[4], Muhammad Khalis Abdul Karim[2*], Aris Doyan[5]

[1]Department of Radiology, Hospital Sultanah Nur Zahirah, Jalan Sultan Mahmud, Kuala Terengganu, Malaysia
[2]Department of Physics, Faculty of Science, Universiti Putra Malaysia, Selangor, Malaysia.
[3]Department of Radiology, School of Medical Sciences, Universiti Sains Malaysia, Kelantan, Malaysia
[4]Department of Radiology, Hospital Sultan Idris Shah, Selangor, Malaysia
[5]Physics Education Program, FKIP, University of Mataram, Lombok Island, West NusaTenggara, Indonesia

Received: December 9, 2025
Revised: January 15, 2026
Accepted: February 3, 2026
Published: February 28, 2026

Corresponding Author*:
Muhammad Khalis Abdul Karim
mkhalis@upm.edu.my

DOI: 10.56566/amplitudo.v5i1.527

Abstract: This study aimed to characterize the relaxivity profiles of pure agarose and gadobutrol in 1% (w/v) agarose under two experimental conditions (within the air and tap-water immersion). T_1 and T_2 values were quantified at 3 Tesla, Siemens, Vida scanner using inversion recovery turbo spin echo (IR-TSE) for T_1 and multi-echo turbo spin echo (ME-TSE) for T_2. Different concentration of agarose (0.2 – 4.0% w/v) and gadobutrol (0.5 – 6.0 mM) and their T_1 and T_2 value for each concentration were measured. Pure agarose demonstrated low longitudinal relaxivity ($r_1 \approx 0.04$ - 0.05 $s^{-1}.(\%w/v)^{-1}$ vs. $r_1 \approx 2.97$ - 3.52 $s^{-1}mM^{-1}$) and high transverse relaxivity ($r_2 \approx 5.00$ - 6.34 $s^{-1}.(\%w/v)^{-1}$ vs. $r_2 \approx 3.80$ - 4.55 $s^{-1}mM^{-1}$) compared to gadobutrol. Agarose showed a very high r_2/r_1 ratio (129.4-160.0) than gadobutrol (1.28-1.29), reflecting stronger gel-matrix effects on transverse dephasing than on longitudinal recovery. Tap-water immersion had shortened T_1 by ≈9% relative to air, without significantly increasing variability. These findings provide relaxivity values for agarose and gadobutrol under well-defined conditions and illustrate how their complementary relaxation behavior can tune T1 and T2 values over a wide range to create customizable MRI calibration phantom for research and clinical use.

Keywords: Agarose gel; Gadobutrol; Quantitative MRI; T_1 relaxivity; T_2 relaxivity

Introduction

Quantitative T_1 mapping has emerged as a powerful MRI biomarker capable of providing objective, reproducible measures of tissue properties in cardiovascular and oncological applications (Barison et al., 2023; Karamitsos & Neubauer, 2022). However, its diagnostic potential can only be fully realised when measurements are standardised across scanners, protocols and across centres. Calibration, quality assurance (QA), and quality control (QC) workflows rely on reference materials whose relaxation properties are stable, well characterised and traceable (Kellman & Hansen, 2014; Taylor et al., 2016). On top of that, the measured value (e.g., T_1, T_2) within the range of human tissue (e.g., myocardium, brain) are essential in QA/ QC in quantitative imaging (Captur et al., 2016; Cerussi et al., 2010; Zhang et al., 2021)

In clinical practice, T_1 and T_2 values remain vulnerable to variability, arising from differences in hardware, acquisition parameters, and reconstruction algorithms (Granitz et al., 2019; Lee et al., 2020; Pachowsky et al., 2013; Razzaq et al., 2024). Such variability complicates longitudinal follow-up, multi-

How to Cite:
Ha', M. C., Kamal, I., Kechik, M. M. A., Sayuti, K. A., Mohammed, Y., Karim, M. K. A., & Doyan, A. (2026). A Comparative Study of Gadobutrol Relaxivity at 3 Tesla for Sustainable Contrast Management and Standardized Phantom Calibration. *AMPLITUDO: Journal of Science and Technology Innovation*, *5*(1), 117–129. https://doi.org/10.56566/amplitudo.v5i1.527

centre studies, and comparison of results across different platforms. For phantom-based QA, calibration, and harmonization, it is therefore essential that reference materials not only stable but also well characterized and tuned to reproducible tissue-like T_1 and T_2 under the same scanner and sequence condition used clinically. A key enabler of this tuning is accurate relaxivity data linking to gel matrices, solute concentration, and relaxation rate that underpins calibration strategies and cross-platform harmonization (Bane et al., 2018; Keenan et al., 2021). In the broader phantom literature, Abdul Karim and co-workers have highlighted the credible phantom should grounded in systematic characterization of materials properties – spanning structural, mechanical, dielectric and attenuation behaviour – so that the constructed model behave predictably in the intended imaging environment (Kamal et al., 2021, 2022). Taken together, these principles support the view that knowing the relaxivity and physical behaviour of phantom constituents allows the relaxation target (T1/T2) to be customize to the capacity and conditions of the specific scanner, strengthening the validity of phantom-based calibration for real world clinical deployment.

Among available materials, agarose gel is a long-standing choice due to its stable matrix, tuneable concentration and tissue-equivalent water content (Captur et al., 2020; McIlvain et al., 2019; Mitchell et al., 1986). Agarose concentration predominantly modulates transverse relaxation (T_2), acting as a T_2 modifier by restricting water mobility and altering microstructural environments (Antoniou & Damianou, 2022). In parallel, gadolinium-based contrast agents such as gadobutrol (Gadovist®, Bayer) have been widely used as T_1 modifiers due to their strong paramagnetic effect on longitudinal relaxation (Keenan et al., 2021). Previous studies have reported gadobutrol relaxivities in blood and plasma at 3 Tesla (Shen et al., 2015; Szomolanyi et al., 2019), and agarose-based relaxometry systems using dopants such as nickel chloride (Captur et al., 2016; Fritz et al., 2024), further underscoring the value of tuneable gel matrices for quantitative MRI calibration.

Despite this body of work, there is comparatively limited systematic evaluation of the combined relaxivity behaviour of agarose-gadobutrol system at 3 Tesla. Prior work has reported gadobutrol relaxivity in biological media (e.g., blood, plasma) or has focused on other dopants in gel system (e.g., Nickel Chloride, soy lecithin), leaving a gap in understanding of how agarose and gadobutrol individually and interactively shape r1 and r2 when the goal is to target a broad, tissue-equivalent T1/T2 design for scanners-specific QA at 3T (Fritz et al., 2024; Marth et al., 2025; Szomolanyi et al., 2019; Vassiliou et al., 2016). A closely related philosophy has been demonstrated by Okada et al., who derived determination equations for phantom T1 and T2 based on measured relaxivities of gel coagulant combined with gadobutrol, illustrating how relaxivity can be treated as a primary, measurable material property that directly enabled controlled phantom design(Okada et al., 2025)

Therefore, the objectives of this study were: (i) to quantify the relaxivity profiles (r_1 and r_2) of pure agarose, and gadobutrol in a fixed 1% (w/v) agarose matrix, across a range of concentrations, and (ii) to assess the influence of scanning environment (air versus tap-water immersion) on T_1 and T_2 measurements. By establishing the r_2/r_1 ratios and environmental sensitivity of these materials at 3 Tesla, this work aims to provide a quantitative framework for using agarose-gadobutrol systems in T_1 and T_2 mapping calibration in the broader context of quantitative MRI.

Method

Sample Preparation

A series of agarose and gadobutrol gel samples were prepared to characterise their relaxivity profiles. Agarose gel (Molecular Biology Grade) was dissolved in distilled water to produce concentrations ranging from 0.2% to 4.0% (w/v), following established procedures for tissue-mimicking gel systems (Antoniou & Damianou, 2022). The mixture was heated to 75 - 95^{0}C under continuous stirring at 350 rpm until fully dissolved and visually homogenous. The solution was then cooled to 40 - 50^{0}C prior to casting into individual containers. For gadobutrol-doped samples, a stock solution of gadobutrol (1mmol/mL; 1000mmol/L) was serially (2-step) diluted according to the standard dilution law (equation 1):

$$C_1 V_1 = C_2 V_2 \quad (1)$$

where C_1 and V_1 are the initial concentration and volume, and C_2 and V_2 are the target concentration and final volume after dilution. For step 1 only involve gadobutrol and distilled water. In step 2 the final volume are including the volume of 1% agarose base matrix. The diluted gadobutrol solutions were combined with 1% (w/v) agarose to produce doped gels spanning 0.5 - 6.0 mmol/L.

In total, 15 samples (A-O) were prepared (Table 1). Samples A-H contained varying agarose concentrations (0.2 - 4.0%) without gadobutrol, while samples I-O consisted of 1% agarose doped with gadobutrol at 0.5-6.0 mmol/L. This design permitted separate evaluation of agarose as a T_2 modifier and gadobutrol as a T_1 modifier, as well as the combined effects of the two components. The preparation step was illustrated in Figure 1.

Table 1. Composition of agarose and gadobutrol gel samples

Sample ID	Agarose % (w/v)	Gadobutrol (mmol/L)
A	0.2	0.0
B	0.3	0.0
C	0.5	0.0
D	0.6	0.0
E	1.0	0.0
F	2.0	0.0
G	3.0	0.0
H	4.0	0.0
I	1.0	0.5
J	1.0	1.0
K	1.0	2.0
L	1.0	3.0
M	1.0	4.0
N	1.0	5.0
O	1.0	6.0

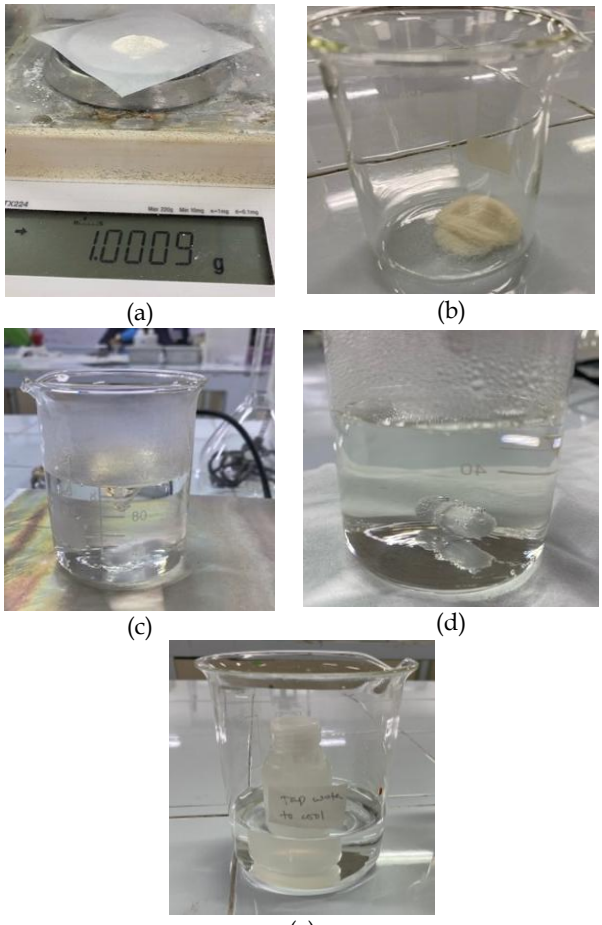

Figure 1. Preparation of the agarose solution: First, weighing agarose powder (a), transferring into a heat resistant beaker (b), dissolving with magnetic stirrer (350 rpm) at 75- 95°C (c), obtaining a homogenous and clear solution (d), cooling (40^{0}C to 50^{0}C) before casting into containers, and casting into containers and cooling using a room-temperature water bath (e) to catalyze the cooling effect to initiate setting from the base and displace any trapped air within the samples. Figure 2 shows the workflow of the methods.

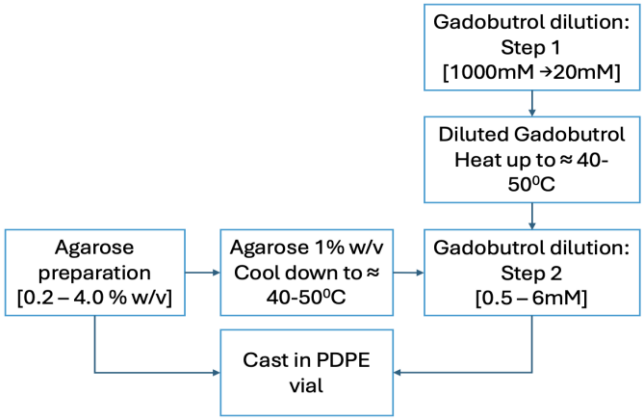

Figure 2. Workflow of the study methodology

MRI Data Acquisition

All imaging was performed on a 3 Tesla MRI system (Magnetom Vida, Siemens Healthineers). Two sequences were used; Inversion Recovery Turbo Spin Echo (IR-TSE) for T_1-weighted imaging and Multi-Echo Turbo Spin Echo (ME-TSE) for T_2-weighted imaging as shown in Table 2.

Table 2. MRI acquisition parameters used for inversion recovery turbo spin echo (IR-TSE) and multi-echo turbo spin echo (ME-TSE) sequences

Parameter	IR-TSE	ME-TSE
TR (ms)	7000	7000
TE (ms)	8.8	8.9, 18, 27, 36, 45, 54, 63, 72, 80
TI (ms)	30, 60, 100, 250, 400, 600, 900,1500, 2000, 3000	Not applicable
FOV read (mm)	260	260
FOV phase (%)	81.3	81.3
Slice thickness (mm)	6	6
Pixel size (mm)	0.8x0.8	0.9x0.9
Distance factor (%)	30	30
No. of slices	3	3
Flip angle (°)	180	180
Base resolution	320	256
Phase resolution (%)	80	75
Acceleration mode	GRAPPA x 2	GRAPPA x 2
Bandwidth (Hz/pixel)	279	279
Acquisition time per TI/ TE (min)	3:32	1:40
Total acquisition time (min)	31:08	15:00

Sequence parameters (e.g. repetition time (TR), echo time (TE), inversion times (TI), echo train length, slice thickness, field of view (FOV), and matrix size) were

selected based on prior work to provide accurate relaxation time estimation while maintaining clinically feasible scan durations. IR-TSE was chosen because it has been shown to produce T_1 values comparable to inversion-recovery spin echo (IR-SE) at 3T, but with shorter acquisition times (Yongabi et al., 2021).

Although geometric matching between the reference T1 and T2 acquisition is desirable, IR-TSE and ME-TSE have different timing and SNR constraints. Therefore, while slice thickness, FOV, and slice prescriptions (orientation and slice location/ centre) were matched between sequences, the in-plane matrix (base resolution) differed slightly to maintain stable fitting performance, particularly for ME-TSE where signal decays substantially at longer TE. Importantly, within each reference measurement (T1 or T2), acquisition setting were kept constant across all samples and scans, except for intended TI/TE sampling.

Experimental Conditions

Relaxivity measurements were conducted under two controlled environmental conditions. First, samples were placed in a container, with no surrounding medium (air-phantom interface). Longitudinal and transverse relaxation rate values and derived relaxivities were denoted R_{1a}, r_{1a} (T_1) and R_{2a}, r_{2a} (T_2). Second, the same samples in the same container were immersed in tap water that was also equilibrated to the scanner's room temperature (18 - 22^{0}C). Longitudinal and transverse relaxation rate values measured under this condition were denoted R_{1w}, r_{1w} (T_1) and R_{2w}, r_{2w} (T_2).

Before scanning, all samples were left to equilibrate with the MRI room temperature (18 - 22^{0}C) to minimise temperature-related variation in T_1 and T_2 values. Sample positions were kept consistent between sequences and conditions to reduce geometric and B_0/B_1 field variations. Representative sample arrangements and magnitude images were documented to support reproducibility.

Relaxivity Analysis

Relaxometry analysis was performed using MATLAB R2024a (MathWorks, Natick, MA, USA). For each sample, regions-of-interest (ROIs) were drawn centrally within the gel to avoid edge artifacts. Mean signal intensities across all inversion times (IR-TSE) and echo times (ME-TSE) were exported for curve fitting. Longitudinal relaxation (T_1) was modelled using the inversion recovery Equation 2.

$$S(TI) = M_0\left(1 - 2e^{-\frac{TI}{T1}}\right) \quad (2)$$

where M_0 is the equilibrium signal and TI is the inversion time. Non-linear least square fitting was used to estimate T_1. Transverse relaxation (T_2) was modelled using mono-exponential decay (Equation 3):

$$S(TE) = S_0 e^{-\frac{TE}{T2}} \quad (3)$$

where S_0 is the initial signal and TE is the echo time. T_2 values were obtained from exponential fits to ME-TSE data. Relaxation rates were defined as $R_1 = 1/T_1$ and $R_2 = 1/T_2$. In the presence of a paramagnetic agent, relaxation was assumed to follow (Equation 4 and 5):

$$R_1 = R_{1,0} + r_1[CA] \quad (4)$$

$$R_2 = R_{2,0} + r_2[CA] \quad (5)$$

where $R_{1,0}$ and $R_{2,0}$ are baseline rates of the undoped medium for each series. The term [CA] is used as a general concentration variable, which each meaning dependent on experimental series. First, gadobutrol series represent gadobutrol concentration in mM and r_1 and r_2 are the longitudinal and transverse relaxivities with units $s^{-1}mM^{-1}$. Second, the agarose series, where agarose is not a paramagnetic agent, but, within the investigated range, [CA] is defined as agarose concentration expressed as %w/v. In this context, r1 and r2 should be interpreted as empirical sensitivity coefficients that describe the change in relaxation rate per unit change in agarose content (unit $s^{-1}.(\%w/v)^{-1}$) rather than relaxivity in the strict contrast agent sense. For each material, linear regression of R_1 and R_2 against concentration was used to derive r_1 and r_2 from the slope of the best-fit line. Relaxivity ratios r_2/r_1 were calculated to characterise the dominant relaxation pathway (T_1- or T_2-weighted behaviour).

Samples were systematically arranged within a container to maintain consistent positioning during scanning (Figure 2a). Representative MRI images of the samples are shown in Figure 2b.

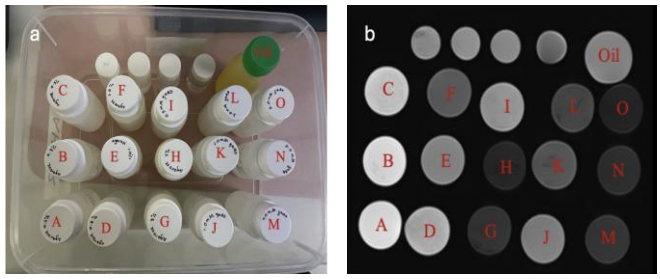

Figure 3. Samples arrangement for MRI scanning: (a) labelled sample placement within the container, and (b) corresponding MRI image of the samples.

Statistical Analysis

The impact of scanning environment (air versus tap-water immersion) on T_1 and T_2 was assessed using

paired statistical tests. Normality of the paired differences was evaluated with the Shapiro-Wilk test. Where normality was satisfied, paired-samples t-tests were used to compare mean T_1 and T_2 values between conditions. When normality assumptions were violated, Wilcoxon signed-rank tests were performed as a non-parametric alternative.

Bias-corrected and accelerated (BCa) 95% bootstrap confidence intervals (CIs) based on 5000 resamples were generated to provide robust estimates of mean differences and to assess the stability of the findings. Effect sizes (Cohen's *d*) were reported for parametric comparisons. Coefficients of variation (CoV) within each ROI were calculated as a measure of measurement stability. Statistical analysis was carried out in SPSS Statistics version 30.0 (IBM Corp., Armonk, NY, USA), and $p < 0.05$ was considered statistically significant.

Result and Discussion

T_1 and T_2 of Agarose-Gadobutrol Gel Samples

Table 3 shows the T_1 and T_2 relaxation times of the agarose-gadobutrol gel samples across different concentrations measured in air and under tap-water immersion. Across the 15 samples, both T_1 and T_2 values showed a clear concentration-dependent decrease with increasing agarose or gadobutrol concentration. In the 1% agarose series doped with gadobutrol, T_1 shortened markedly from approximately 2197.17 ± 111.46 ms (0 mmol/L Gd) to 52.86 ± 0.23 ms at 6 mmol/L, consistent with the strong paramagnetic effect of gadolinium chelates on longitudinal relaxation. Notably, the 0mM gadobutrol condition corresponds to the 1% agarose matrix baseline, and its T_1 and T_2 values define the intercept terms $R_{1,0}$ and $R_{2,0}$ used in the subsequent relaxivity egressions. Similar monotonic decreases were observed for T_2, reflecting the combined influence of matrix-induced water restriction and paramagnetic relaxation enhancement.

Table 3. T1 and T2 values of agarose-gadobutrol gel samples at varying concentrations, measured under two scanning environments

Sample ID	Concentration		In the air		Tap-water immersion	
	Agarose (% w/v)	Gd (mmol/L)	T1 value	T2 value	T1 value	T2 value
A	0.2	0	2299.36 ±116.36	760.82 ±20.35	2084.32 ±83.51	575.04 ±10.68
B	0.3	0	2300.10 ±100.12	741.90 ±62.89	2139.25 ±123.90	575.81 ±19.38
C	0.5	0	2093.49 ±213.71	306.02 ±9.42	2015.88 ±87.43	280.00 ±6.52
D	0.6	0	2230.11 ±109.39	253.83 ±11.55	2030.13 ±90.20	243.84 ±1.14
E	1	0	2197.17 ±111.46	155.07 ±2.68	1975.59 ±89.77	163.55 ±0.29
F	2	0	2001.83 ±104.70	80.00 ±1.00	1837.28 ±91.91	81.29 ±0.80
G	3	0	1850.40 ±124.35	49.83 ±1.32	1704.57 ±110.69	52.88 ±0.71
H	4	0	1745.73 ±111.68	40.58 ±0.92	1480.51 ±57.68	45.55 ±0.02
I	1	0.5	464.05 ±2.34	121.33 ±1.24	402.25 ±4.71	116.91 ±0.60
J	1	1	261.23 ±1.72	98.04 ±0.92	221.44 ±0.75	93.57 ±0.83
K	1	2	138.84 ±0.37	69.67 ±0.48	116.22 ±0.88	64.54 ±0.34
L	1	3	100.90 ±0.16	54.70 ±0.55	83.32 ±0.35	48.61 ±0.10
M	1	4	77.39 ±0.47	44.39 ±0.11	64.16 ±0.17	40.09 ±0.17
N	1	5	65.37 ±0.29	40.83 ±0.28	53.87 ±0.17	35.15 ±0.02
O	1	6	52.86 ±0.23	33.78 ±0.10	45.49 ±0.29	29.56 ±0.09

*T1/T2 value = mean±SD (ms)

This behavior aligns with classical relaxation theory, where increasing macromolecular content or paramagnetic ion concentration reduces the correlation time of water protons and increases relaxation rates (Fullerton et al., 1986; Granato et al., 2018). In agarose gels, higher polymer concentrations restrict water mobility, while gadobutrol introduces local magnetic field fluctuations that predominantly shorten T_1 but also affect T_2 (Antoniou & Damianou, 2022; Caccavo et al., 2017; Mitchell et al., 1986).

A minor methodological limitation is that the in-plane resolution differed slightly between the reference IR-TSE (T_1) and ME-TSE (T_2) acquisitions due to sequence-specific constraints. However, because measurements were performed in homogeneous phantom regions using matched slice prescription and central ROIs, the influence of partial volume effects is expected to be minimal (Blaszczyk et al., 2017; Dalmer et al., 2024). Future work will standardize in-plane solution across reference sequences where feasible.

Relaxivity of Pure Agarose

The relaxivity analysis for pure agarose demonstrated a low longitudinal relaxivity and a high transverse relaxivity. Under air conditions, the mean r_1 was approximately 0.0352 $s^{-1}.(\%w/v)^{-1}$, increasing slightly to 0.0487 $s^{-1}.(\%w/v)^{-1}$ under tap-water immersion. In contrast, r_2 was substantially higher at around 6.3433 $s^{-1}.(\%w/v)^{-1}$ in air and 5.6015 $s^{-1}.(\%w/v)^{-1}$ in water. Linear regression plots of R_1 and R_2 versus agarose concentration confirmed good linearity, particularly for R_2, indicating a robust T_2-dominated effect.

The very low r_1 and high r_2 values highlight agarose's role as a T_2 modifier, exerting relatively modest influence on T_1, but a strong impact on T_2 (Dwihapsari et al., 2020). The resulting r_2/r_1 ratios exceeded 100 across conditions, consistent with previous reports of strong T_2 dependence on agarose content in gel systems (Antoniou & Damianou, 2022; Fritz et al., 2024; Mitchell et al., 1986).

From a relaxivity perspective, this means that agarose concentration can be used primarily to modulate T_2, with limited perturbation of T_1 when concentrations are selected within a biologically relevant range. Representative linear regression plots of $1/T_1$ and $1/T_2$ versus agarose concentration are shown in Figure 3, confirming the strong T_2 dependence of agarose. Table 4 summarises the r_1 and r_2 values of the agarose-only gel samples across the three slices, together with the slice-averaged mean relaxivities for each environment.

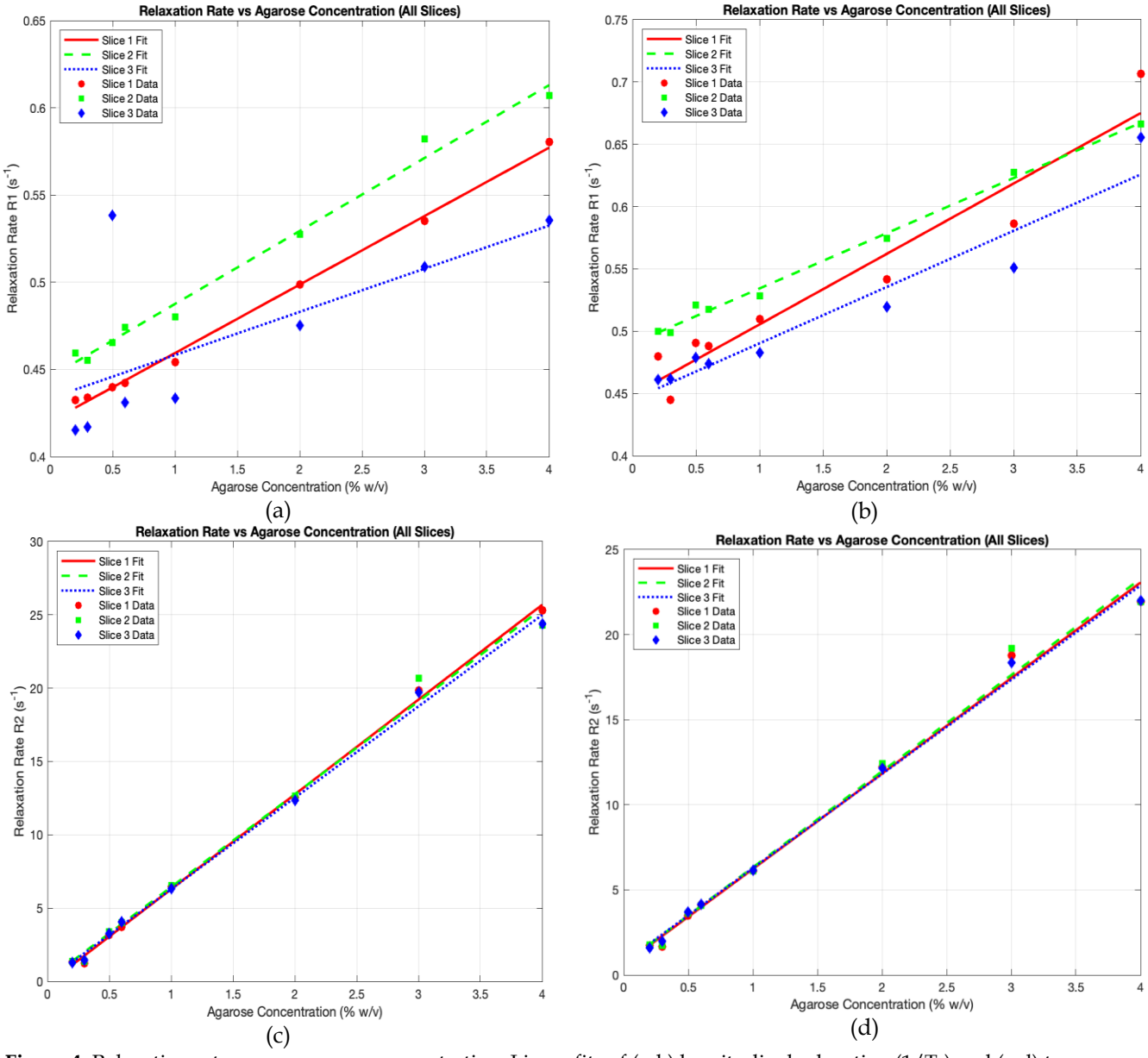

Figure 4. Relaxation rate versus agarose concentration. Linear fits of (a-b) longitudinal relaxation ($1/T_1$) and (c-d) transverse relaxation ($1/T_2$) for phantoms measured in room air and in tap-water immersion.

Table 4. Relaxivity values of agarose gel samples measured in room air (a) and tap-water immersion (w).

Phantom	r1_a ($s^{-1}.\%^{-1}$ w/v)	r1_w ($s^{-1}.\%^{-1}$ w/v)	r2_a ($s^{-1}.\%^{-1}$ w/v)	r2_w ($s^{-1}.\%^{-1}$ w/v)
Agarose_Slice1	0.0392	0.0565	6.4649	5.6113
Agarose_Slice2	0.0418	0.0443	6.3291	5.6533
Agarose_Slice3	0.0247	0.0452	6.2358	5.5398
mean	0.0352	0.0487	6.3433	5.6015

Table 4 also shows inter-slice variability, most evidence for agarose r_1, where slice to slice differences were larger than r_2. This likely reflects a combination of modest spatial heterogeneity (e.g., local gel concentration/ structure), ROI positioning sensitivity and residual B_0/B_1 non-uniformity across the phantom volume. Importantly, despite this variability in T_1, overall patterns remain consistent: agarose exhibit low longitudinal and high transverse sensitivity, yielding a persistently high r_2/r_1 ratios across slices. Therefore, the main conclusion – agarose acting primarily as a T2 modifier within the investigated range – remained unchanged.

Relaxivity of Gadobutrol in 1% Agarose

In contrast to agarose, gadobutrol incorporated into 1% agarose produced high longitudinal relaxivity and moderate transverse relaxivity. Under air conditions, r_1 was approximately 2.975 $s^{-1}.mM^{-1}$ and r_2 about 3.801 $s^{-1}.mM^{-1}$. In tap-water immersion, r_1 increased to around 3.524 $s^{-1}.mM^{-1}$ while r_2 rose to 4.548 $s^{-1}.mM^{-1}$. Linear regression of R_1 and R_2 versus gadobutrol concentration showed strong linearity, confirming that the relaxivity model adequately described the concentration-relaxation relationship. The r_2/r_1 ratios for gadobutrol in 1% agarose were close to unity (approximately 1.28-1.29), indicating a more balanced influence on T_1 and T_2 but with a dominant role in enhancing longitudinal relaxation(Hamzaini et al., 2024; Kang et al., 2018). These values are consistent with prior work demonstrating that gadobutrol possesses relatively high T_1 relaxivity among macrocyclic gadolinium agents at 3T (Szomolanyi et al., 2019), making it a suitable choice when strong T_1 sensitivity is required.

Taken together, the complementary relaxivity behaviors of agarose and gadobutrol indicate that agarose concentration can be adjusted to control T_2, while gadobutrol concentration primarily tunes T_1. This separability is advantageous for quantitative calibration schemes in which specific T_1 and T_2 values need to be targeted over a defined range, since it allows systematic exploration of contrast behaviour and mapping performance across known relaxation regimes (Boursianis et al., 2021; Hajidah & Dwihapsari, 2021; Kang et al., 2018). Linear regression analysis demonstrated good agreement between measured relaxation rates and gadobutrol concentration (Figure 4), confirming gadobutrol's effectiveness as a T_1-active component within an agarose matrix. Table 5 presents the corresponding relaxivity values for gadobutrol in a 1% agarose matrix, again reported for each slice and as mean values, allowing direct comparison between agarose and gadobutrol and between the two measurement conditions.

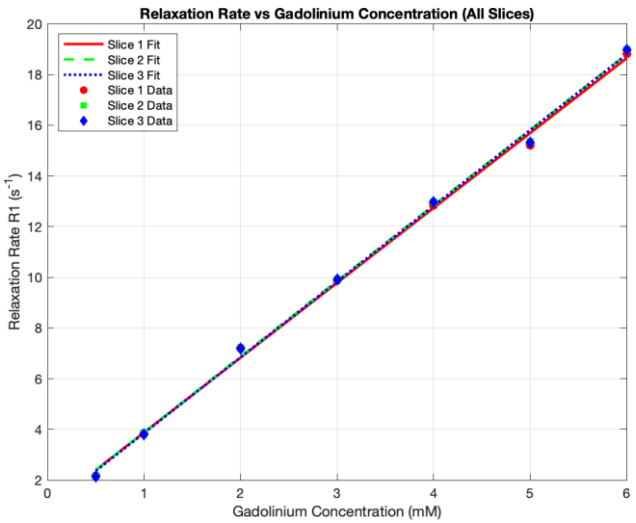

(a)

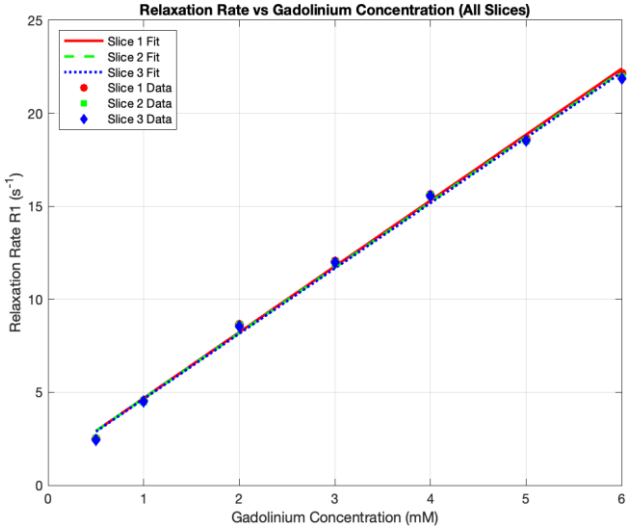

(b)

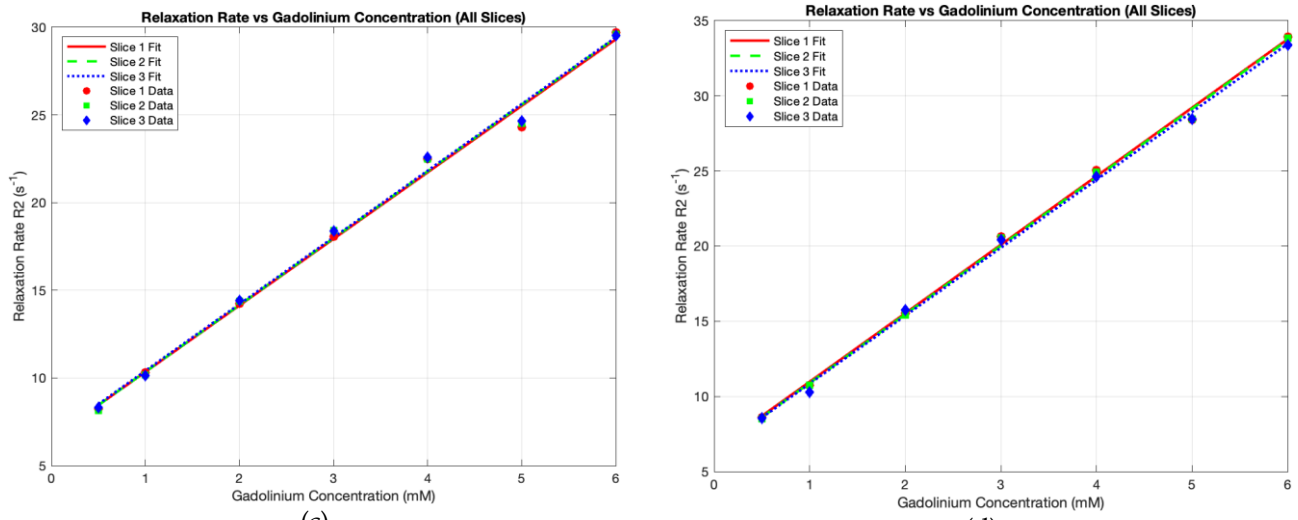

Figure 5: Relaxation rate versus gadobutrol concentration in 1% agarose. Linear fits of (a-b) longitudinal relaxation ($1/T_1$) and (c-d) transverse relaxation ($1/T_2$) for sample measured in room air and in tap-water immersion.

Table 5. Relaxivity values of gadobutrol in 1% agarose measured in room air (a) and tap-water immersion (w).

Phantom	r1_a ($s^{-1}.mM^{-1}$)	r1_w ($s^{-1}.mM^{-1}$)	r2_a ($s^{-1}.mM^{-1}$)	r2_w ($s^{-1}.mM^{-1}$)
Gd_Slice1	2.9540	3.5441	3.7928	4.5593
Gd_Slice2	2.9827	3.5166	3.8083	4.5630
Gd_Slice3	2.9877	3.5109	3.8026	4.5208
mean	2.9748	3.5239	3.8012	4.5477

Relaxivity Ratio (r_2/r_1) and Implications for T_1/T_2 Calibration

The comparison of relaxivity ratios underscores the distinct functional roles of the two materials. For agarose, r_2/r_1 values in the range of 129.39-160.00 confirm that it is predominantly a T_2 driver, inducing large changes in transverse relaxation for relatively small changes in T_1. For gadobutrol in 1% agarose, $r_2/r_1 \approx 1.28$ - 1.29 indicates nearly equal contributions to both relaxation pathways but with a primary purpose of shortening T_1.

From a design perspective, this dual-modifier system offers a flexible, mechanistically transparent framework. First, T_2 tailoring is achieved by adjusting agarose concentration while keeping gadobutrol constant or absent. Second, T_1 tailoring is achieved by varying gadobutrol concentration in a fixed, low to moderate agarose matrix (e.g., 1% w/v).

By combining the measured relaxivities with desired T_1 and T_2 targets, one can theoretically determine the required agarose and gadobutrol concentrations for specific relaxation properties (Fritz & Schick, 2025; Hattori et al., 2013; Ikemoto et al., 2011; Okada et al., 2025). This provides a rational alternative to empirical trial-and-error approaches and supports reproducible calibration for quantitative MRI applications such as T_1 and T_2 mapping. Table 6 summarises these r_2/r_1 ratios for agarose and gadobutrol, highlighting the markedly higher T_2-dominated behaviour of agarose compared with the more balanced relaxivity profile of gadobutrol in 1% agarose.

Table 6. Relaxivity ratio (r2/r1) of agarose and gadobutrol gels under different experimental conditions.

Material	r2/r1 (Air)	r2/r1 (Water)
Agarose (0.2-4.0% w/v)	180.17	115.02
Gadobutrol (0.5-6.0mmol/L in 1% agarose)	1.28	1.29

The agarose r_2/r_1 ratio decreased substantially under tap-water immersion (Table 6). This reduction is primarily driven by a proportionally larger increase in r_1 than decrease in r_2 indicating that longitudinal relaxation sensitivity becomes more efficient in the aqueous environment while transverse relaxivity is slightly reduced. Practically, this means that, immersion condition can shift the relative T_2-dominant character of agarose, reinforcing the need to report and standardized environmental conditions when using agarose-based phantoms for cross-study or longitudinal calibration. One plausible contributing mechanism is magnetization transfer (MT). Agarose gels contain a semi-solid macromolecular pool that exchanges magnetization with the free-water pool. Routine RF pulse train can

partially saturate the macromolecular pool and transfer this saturation to free water, which tends to increase the apparent R_1 (shorten the apparent T_1)(Jones et al., 2013; Varma et al., 2018). Importantly, MT does not only "exist" under immersion, but the degree to which MT contaminates the measured apparent T_1 (and thus r_1) can change when the phantom is immersed, because the surrounding conductive/ high-permittivity water alters coil loading and transmit conditions, potentially modifying the effective RF saturation history and spatial B1 distribution experienced by the gel(Brink et al., 2023; Lakshmanan et al., 2020; Ruello & Lattanzi, 2022; Vaidya et al., 2018). If immersion increases the effective saturation experienced by the bound pool, MT will preferentially elevate the measured r_1 more than r_2, providing a physically consistent explanation for the observed drop in r_2/r_1. Overall, the markedly higher r_2/r_1 of agarose compared with gadobutrol supports an orthogonal control strategy, where agarose predominantly drives T_2 while gadobutrol primarily tune T_1. This separation is desirable for quantitative MRI phantoms because it enables more independent spanning of clinically relevant T_1/T_2 combinations rather than forcing both parameters to change together.

Effect of Scanning Environment (Air vs Tap-Water Immersion)

Environmental conditions had a measurable impact on T_1, and a smaller, non-significant effect on T_2. Across 15 paired samples, immersion in tap water reduced T_1 values by an average of -108.30 ms (SE = 22.8; $p < 0.001$), corresponding to an approximate 9.1% reduction relative to scanning in air (mean $T_1 \approx 1191.9$ ms in air). Effect size was large (Cohen's d = 1.12), and similar reductions were observed across three repeated runs, with bootstrap 95% CIs that did not cross zero. For T_2, tap-water immersion also tended to reduce relaxation times by approximately 25 - 31 ms, but these differences did not reach statistical significance (p = 0.105). Within-ROI CoVs were slightly lower in the immersion condition (mean difference -0.57 percentage points), suggesting that water immersion did not compromise, and may slightly improve, measurement stability. The transverse behaviour showed a consistent direction that differed by materials. For agarose, $r_{2,w}$ was consistently lower than $r_{2,a}$ (Table 4 and 6), suggesting that immersion improves macroscopic susceptibility matching at the sample boundary and increase B0 homogeneity, thereby reducing dephasing contribution that would otherwise inflate transverse decay. In contrast, gadobutrol showed higher $r_{2,w}$ than $r_{2,a}$ (Table 5), mirroring the increase observed for r1, and is consistent with medium-dependent relaxation enhancement where water accessibility and molecular motion can modulate relaxation efficiency. In previous study, measuring gadobutrol relaxivity in different protein concentration found that gadobutrol r1 and r2 relaxivities increase with higher concentration of plasma protein (Goetschi et al., 2014) can be basis on explaining the reason of the higher gadobutrol relaxivities in water than air observed in this study. Although net change in T2 did not reach statistical significance in this dataset, the material dependent of r2 changes indicate that environmental control is not neutral and should be standardized when comparing relaxivities values across experiment.

The shortening of T_1 with water immersion is plausible for two reasons. First, tap-water contains dissolved ions that can contribute to relaxation effects, shortening both T_1 and T_2 compared with pure distilled water (Yusuff et al., 2024). Second, immersion reduces susceptibility mismatch at the phantom boundary compared with an air-gel interface, potentially reducing B_0 inhomogeneity and leading to more efficient inversion and recovery processes. These findings are consistent with previous reports emphasizing the influence of immersion media and temperature on relaxation properties of calibration materials (Statton et al., 2022; Vassiliou et al., 2016). They highlight the need to standardize not only material composition but also environmental conditions—such as the use of deionised versus tap-water, careful removal of air bubbles and tight temperature control—when performing relaxivity measurements and quantitative T_1/T_2 calibration.

Future work should evaluate long-term stability and batch-to-batch reproducibility of agarose-gadobutrol gels, validates relaxivity estimates across different MRI platforms and sequences, and refine calibration protocols by standardizing environmental conditions to support robust multi-center quantitative MRI quality assurance.

Conclusion

This study characterized the relaxivity profiles of pure agarose and gadobutrol in 1% agarose at 3 Tesla MRI under two controlled environments (air and tap-water immersion). Pure agarose showed low longitudinal relaxivity ($r_1 \approx 0.04 – 0.05$ $s^{-1}.(\%w/v)^{-1}$) and high transverse relaxivity ($r_2 \approx 5.60 – 6.34$ $s^{-1}.(\%w/v)^{-1}$) yielding a markedly high r_2/r_1 ratios (≈ 115 - 180) consistent with a T_2 modifier. Whereas gadobutrol in 1% agarose exhibited high longitudinal relaxivity ($r_1 \approx 2.95 – 3.52$ $s^{-1}.mM^{-1}$) with moderate transverse relaxivity $r_2 \approx 3.79 – 4.59$ $s^{-1}.mM^{-1}$) and a near unity ratio ($r_2/r_1 \approx 1.29 – 1.29$), supporting its role as a T_1 dominant modifier in this matrix. Environmental conditions influenced both measured relaxation times and relaxivity coefficients, including higher gadobutrol r_1 under immersion

($r_{1,w}>r_{1,a}$) and lower agarose r_2 in water ($r_{2,w}<r_{2,a,}$), alongside an overall ~9% reduction in measured T1 with tap water immersion, emphasizing that surrounding medium should be standardised for quantitative relaxivity studies and phantom calibration. Collectively, the complementary relaxivity profiles provide a rational basis for designing agarose-gadobutrol gel phantoms with more independently tuneable T1 and T2 properties to support quantitative MRI calibration and cross-scanner harmonisation.

Acknowledgments
The authors would like to thank the Cardiac Radiology Unit, Hospital Sultan Idris Shah (HSIS), all collaborators involved in the phantom experiments, and the Ceramics and Ultrasonic Research Laboratory (CURL), Universiti Putra Malaysia (UPM), for providing technical support and access to MRI facilities.

Author Contributions
Conceptualization, M.C.H. and M.K.A.K.; methodology, M.C.H., A.D and I.K.; software and gata processing, I.K.; validation, M.C.H. and M.K.A.K.; formal analysis, M.C.H. and I.K.; investigation, M.C.H.; resources, M.K.A.K; data curation, M.C.H. and I.K.; writing-original draft preparation, M.C.H. and I.K.; writing-review and editing, M.K.A.K.and A.D; visualization, I.K.; supervision, M.K.A.K.; project administration, M.K.A.K. All authors have read and agreed to the published version of the manuscript.

Funding
The Universiti Putra Malaysia financially supported this work through the Geran Putra Berimpak (vot: 9810400). The author would like to acknowledge financial support from the Ministry of Health Malaysia through the Hadiah Latihan Persekutuan (HLP) scholarship.

Conflicts of Interest
The authors declare no conflict of interest.

References

Antoniou, A., & Damianou, C. (2022). MR relaxation properties of tissue-mimicking phantoms. *Ultrasonics*, *119*. https://doi.org/10.1016/j.ultras.2021.106600

Bane, O., Hectors, S. J., Wagner, M., Arlinghaus, L. L., Aryal, M. P., Cao, Y., Chenevert, T. L., Fennessy, F., Huang, W., Hylton, N. M., Kalpathy-Cramer, J., Keenan, K. E., Malyarenko, D. I., Mulkern, R. V., Newitt, D. C., Russek, S. E., Stupic, K. F., Tudorica, A., Wilmes, L. J., … Taouli, B. (2018). Accuracy, repeatability, and interplatform reproducibility of T1 quantification methods used for DCE-MRI: Results from a multicenter phantom study. *Magnetic Resonance in Medicine*, *79*(5), 2564–2575. https://doi.org/10.1002/mrm.26903

Barison, A., Martini, N., Dellegrottaglie, S., & Pontone, G. (2023). *Introduction to Cardiac MRI* (p. 11). https://doi.org/10.1007/978-3-031-32593-9_1

Blaszczyk, E., Töpper, A., Schmacht, L., Wanke, F., Greiser, A., Schulz-Menger, J., & von Knobelsdorff-Brenkenhoff, F. (2017). Influence of spatial resolution and contrast agent dosage on myocardial T1 relaxation times. *Magnetic Resonance Materials in Physics, Biology and Medicine*, *30*(1), 85–91. https://doi.org/10.1007/s10334-016-0581-0

Boursianis, T., Kalaitzakis, G., Pappas, E., Karantanas, A. H., & Maris, T. G. (2021). MRI diffusion phantoms: ADC and relaxometric measurement comparisons between polyacrylamide and agarose gels. *European Journal of Radiology*, *139*, 109696. https://doi.org/10.1016/j.ejrad.2021.109696

Brink, W. M., Remis, R. F., & Webb, A. G. (2023). Radiofrequency safety of high permittivity pads in MRI—Impact of insulation material. *Magnetic Resonance in Medicine*, *89*(5), 2109–2116. https://doi.org/10.1002/mrm.29580

Caccavo, D., Cascone, S., Poto, S., Lamberti, G., & Barba, A. A. (2017). Mechanics and transport phenomena in agarose-based hydrogels studied by compression-relaxation tests. *Carbohydrate Polymers*, *167*, 136–144. https://doi.org/10.1016/j.carbpol.2017.03.027

Captur, G., Bhandari, A., Brühl, R., Ittermann, B., Keenan, K. E., Yang, Y., Eames, R. J., Benedetti, G., Torlasco, C., Ricketts, L., Boubertakh, R., Fatih, N., Greenwood, J. P., Paulis, L. E. M., Lawton, C. B., Bucciarelli-Ducci, C., Lamb, H. J., Steeds, R., Leung, S. W., … Moon, J. C. (2020). T 1 mapping performance and measurement repeatability: Results from the multi-national T 1 mapping standardization phantom program (T1MES). *Journal of Cardiovascular Magnetic Resonance*, *22*(1). https://doi.org/10.1186/s12968-020-00613-3

Captur, G., Gatehouse, P., Keenan, K. E., Heslinga, F. G., Bruehl, R., Prothmann, M., Graves, M. J., Eames, R. J., Torlasco, C., Benedetti, G., Donovan, J., Ittermann, B., Boubertakh, R., Bathgate, A., Royet, C., Pang, W., Nezafat, R., Salerno, M., Kellman, P., & Moon, J. C. (2016). A medical device-grade T1 and ECV phantom for global T1 mapping quality assurance—The T1 Mapping and ECV Standardization in cardiovascular magnetic resonance (T1MES) program. *Journal of Cardiovascular Magnetic Resonance*, *18*(1), 58–58. https://doi.org/10.1186/s12968-016-0280-z

Cerussi, A., Durkin, A., Kwong, R., Quang, T., Hill, B., Tromberg, B. J., MacKinnon, N., & Mantulin, W. W. (2010). *Quality control and assurance for validation of DOS/I measurements* (R. J. Nordstrom, Ed.; p. 756703). https://doi.org/10.1117/12.842755

Dalmer, A., Meinel, F. G., Böttcher, B., Manzke, M., Lorbeer, R., Weber, M.-A., Baeßler, B., & Klemenz, A.-C. (2024). Native myocardial T1 mapping: Influence of spatial resolution on quantitative results and reproducibility. *Quantitative Imaging in Medicine and Surgery*, *14*(1), 20–30. https://doi.org/10.21037/qims-23-943

Dwihapsari, Y., Asdiantoro, E., & Maulidiyah, N. (2020). T2 Quantification of Agarose with Contrast Agent in Magnetic Resonance Imaging. *Journal of Physics: Conference Series*, *1505*(1), 012044. https://doi.org/10.1088/1742-6596/1505/1/012044

Fritz, V., Eisele, S., Martirosian, P., Machann, J., & Schick, F. (2024). A straightforward procedure to build a non-toxic relaxometry phantom with desired T1 and T2 times at 3T. *Magnetic Resonance Materials in Physics, Biology and Medicine*, *37*(5), 899–907. https://doi.org/10.1007/s10334-024-01166-7

Fritz, V., & Schick, F. (2025). Recipe for Hydrogels With Tunable Relaxation and Diffusion Properties for Use as MRI Test Materials. *Magnetic Resonance in Medicine*, mrm.70120. https://doi.org/10.1002/mrm.70120

Fullerton, G. D., Ord, V. A., & Cameron, I. L. (1986). An evaluation of the hydration of lysozyme by an NMR titration method. *Biochimica et Biophysica Acta (BBA) - Protein Structure and Molecular Enzymology*, *869*(3), 230–246. https://doi.org/10.1016/0167-4838(86)90063-4

Goetschi, S., Froehlich, J. M., Chuck, N. C., Curcio, R., Runge, V. M., Andreisek, G., Nanz, D., & Boss, A. (2014). The Protein and Contrast Agent–Specific Influence of Pathological Plasma-Protein Concentration Levels on Contrast-Enhanced Magnetic Resonance Imaging: *Investigative Radiology*, *49*(9), 608–619. https://doi.org/10.1097/RLI.0000000000000061

Granato, L., Vander Elst, L., Henoumont, C., Muller, R. N., & Laurent, S. (2018). Optimizing Water Exchange Rates and Rotational Mobility for High-Relaxivity of a Novel Gd- DO 3A Derivative Complex Conjugated to Inulin as Macromolecular Contrast Agents for MRI. *Chemistry & Biodiversity*, *15*(2), e1700487. https://doi.org/10.1002/cbdv.201700487

Granitz, M., Motloch, L. J., Granitz, C., Meissnitzer, M., Hitzl, W., Hergan, K., & Schlattau, A. (2019). Comparison of native myocardial T1 and T2 mapping at 1.5T and 3T in healthy volunteers. *Wiener Klinische Wochenschrift*, *131*(7–8), 143–155. https://doi.org/10.1007/s00508-018-1411-3

Hajidah, D. H., & Dwihapsari, Y. (2021). *Quantitative T2 magnetic resonance imaging: Analysis of the effect of echo time on images and signal to noise ratio on agarose*. 040003. https://doi.org/10.1063/5.0048234

Hamzaini, N. N., Ghazali, S. A., Yusoff, A. N., Mohd Zaki, F., Wan Sulaiman, W. N. A., & Dwihapsari, Y. (2024). FeCl3 and GdCl3 solutions as superfast relaxation modifiers for agarose gel: A quantitative analysis. *Magnetic Resonance Materials in Physics, Biology and Medicine*, *38*(1), 141–160. https://doi.org/10.1007/s10334-024-01216-0

Hattori, K., Ikemoto, Y., Takao, W., Ohno, S., Harimoto, T., Kanazawa, S., Oita, M., Shibuya, K., Kuroda, M., & Kato, H. (2013). Development of MRI phantom equivalent to human tissues for 3.0-T MRI. *Medical Physics*, *40*(3), 032303. https://doi.org/10.1118/1.4790023

Ikemoto, Y., Takao, W., Yoshitomi, K., Ohno, S., Harimoto, T., Kanazawa, S., Shibuya, K., Kuroda, M., & Kato, H. (2011). Development of a human-tissue-like phantom for 3.0-T MRI. *Medical Physics*, *38*(11), 6336–6342. https://doi.org/10.1118/1.3656077

Jones, C. K., Huang, A., Xu, J., Edden, R. A. E., Schär, M., Hua, J., Oskolkov, N., Zacà, D., Zhou, J., McMahon, M. T., Pillai, J. J., & Van Zijl, P. C. M. (2013). Nuclear Overhauser enhancement (NOE) imaging in the human brain at 7T. *NeuroImage*, *77*, 114–124. https://doi.org/10.1016/j.neuroimage.2013.03.047

Kamal, I., Karim, M. K. A., Harun, H. H., Abdul Razak, H. R., Jian, L. Y., Chyi, J. L. Y., & Kechik, M. M. A. (2021). Evaluation of radiation attenuation properties on a various composition of polydimethylsiloxane (PDMS) for fabrication of kidney phantom. *Radiation Physics and Chemistry*, *189*, 109661. https://doi.org/10.1016/j.radphyschem.2021.109661

Kamal, I., Razak, H. R. A., Abdul Karim, M. K., Mashohor, S., Liew, J. Y. C., Low, Y. J., Zaaba, N. A., Norkhairunnisa, M., & Rafi, N. A. S. M. (2022). Mechanical and Imaging Properties of a Clinical-Grade Kidney Phantom Based on Polydimethylsiloxane and Elastomer. *Polymers*, *14*(3), 535. https://doi.org/10.3390/polym14030535

Kang, K. M., Choi, S. H., Hwang, M., Yun, T. J., Kim, J., & Sohn, C.-H. (2018). T1 Shortening in the Globus Pallidus after Multiple Administrations of Gadobutrol: Assessment with a Multidynamic Multiecho Sequence. *Radiology*, *287*(1), 258–266. https://doi.org/10.1148/radiol.2017162852

Karamitsos, T., & Neubauer, S. (2022). *Cardiovascular magnetic resonance imaging*. 372–378.

Keenan, K. E., Gimbutas, Z., Dienstfrey, A., Stupic, K. F., Boss, M. A., Russek, S. E., Chenevert, T. L., Prasad, P. V., Guo, J., Reddick, W. E., Cecil, K. M., Shukla-

Dave, A., Nunez, D. A., Konar, A. S., Liu, M. Z., Jambawalikar, S. R., Schwartz, L. H., Zheng, J., Hu, P., & Jackson, E. F. (2021). Multi-site, multi-platform comparison of MRI T1 measurement using the system phantom. *PLoS ONE*, *16*(6 June). https://doi.org/10.1371/journal.pone.0252966

Kellman, P., & Hansen, M. (2014). T1-mapping in the heart: Accuracy and precision. *Journal of Cardiovascular Magnetic Resonance*, *16*(1), 2–2. https://doi.org/10.1186/1532-429x-16-2

Lakshmanan, K., Walczyk, J., Brown, R., Rupprecht, S., Yang, Q. X., Lanagan, M. T., & Collins, C. (2020). *Improved brain imaging with a head array with integrated high-permittivity material*. 020077. https://doi.org/10.1063/5.0034556

Lee, E., Kim, P. K., Choi, B. W., & Jung, J. I. (2020). Phantom-Validated Reference Values of Myocardial Mapping and Extracellular Volume at 3T in Healthy Koreans. *Investigative Magnetic Resonance Imaging*, *24*(3), 141–141. https://doi.org/10.13104/imri.2020.24.3.141

Marth, T., Froehlich, J. M., Nanz, D., & Sutter, R. (2025). Gadolinium concentration dependent signal enhancement profiles using routine clinical sequences with gadopiclenol, gadoterate, gadobutrol, and gadoxetate at 1.5, 3 and 7 Tesla. *European Journal of Radiology*, *191*, 112322. https://doi.org/10.1016/j.ejrad.2025.112322

McIlvain, G., Ganji, E., Cooper, C., Killian, M. L., Ogunnaike, B. A., & Johnson, C. L. (2019). Reliable preparation of agarose phantoms for use in quantitative magnetic resonance elastography. *Journal of the Mechanical Behavior of Biomedical Materials*, *97*, 65–73. https://doi.org/10.1016/j.jmbbm.2019.05.001

Mitchell, M. D., Kundel, H. L., Axel, L., & Joseph, P. M. (1986). Agarose as a tissue equivalent phantom material for NMR imaging. *Magnetic Resonance Imaging*, *4*(3), 263–266. https://doi.org/10.1016/0730-725X(86)91068-4

Okada, H., Koori, N., Shimizu, H., Yamamoto, S., Komatsuzaki, T., Fuse, H., Sasaki, K., Miyakawa, S., Yasue, K., & Takahashi, M. (2025). Development of estimation method for T1 and T2 values using the relaxivity of contrast agent and coagulant for a magnetic resonance imaging phantom. *Radiological Physics and Technology*, *18*(2), 469–476. https://doi.org/10.1007/s12194-025-00900-7

Pachowsky, M. L., Trattnig, S., Apprich, S., Mauerer, A., Zbyn, S., & Welsch, G. H. (2013). Impact of different coils on biochemical T2 and T2* relaxation time mapping of articular patella cartilage. *Skeletal Radiology*, *42*(11), 1565–1572. https://doi.org/10.1007/s00256-013-1699-z

Razzaq, S., Haririsanati, L., Eyre, K., Garg, R., Chetrit, M., & Friedrich, M. G. (2024). Inter-scanner comparability of Z-scores for native myocardial T1 and T2 mapping. *Journal of Cardiovascular Magnetic Resonance*, *26*(1), 100004–100004. https://doi.org/10.1016/J.JOCMR.2023.100004

Ruello, G., & Lattanzi, R. (2022). A Physical Framework to Interpret the Effects of High Permittivity Materials on Radiofrequency Coil Performance in Magnetic Resonance Imaging. *IEEE Transactions on Biomedical Engineering*, *69*(11), 3278–3287. https://doi.org/10.1109/TBME.2022.3165763

Shen, Y., Goerner, F. L., Snyder, C., Morelli, J. N., Hao, D., Hu, D., Li, X., & Runge, V. M. (2015). T1 Relaxivities of Gadolinium-Based Magnetic Resonance Contrast Agents in Human Whole Blood at 1.5, 3, and 7 T: *Investigative Radiology*, *50*(5), 330–338. https://doi.org/10.1097/RLI.0000000000000132

Statton, B. K., Smith, J., Finnegan, M. E., Koerzdoerfer, G., Quest, R. A., & Grech-Sollars, M. (2022). Temperature dependence, accuracy, and repeatability of T_1 and T_2 relaxation times for the ISMRM/NIST system phantom measured using MR fingerprinting. *Magnetic Resonance in Medicine*, *87*(3), 1446–1460. https://doi.org/10.1002/mrm.29065

Szomolanyi, P., Rohrer, M., Frenzel, T., Noebauer-Huhmann, I. M., Jost, G., Endrikat, J., Trattnig, S., & Pietsch, H. (2019). Comparison of the Relaxivities of Macrocyclic Gadolinium-Based Contrast Agents in Human Plasma at 1.5, 3, and 7 T, and Blood at 3 T. *Investigative Radiology*, *54*(9), 559–564. https://doi.org/10.1097/RLI.0000000000000577

Taylor, A., Salerno, M., Dharmakumar, R., & Jerosch-Herold, M. (2016). T1 Mapping: Basic Techniques and Clinical Applications. *JACC. Cardiovascular Imaging*, *9*(1), 67–81. https://doi.org/10.1016/j.jcmg.2015.11.005

Vaidya, M. V., Deniz, C. M., Collins, C. M., Sodickson, D. K., & Lattanzi, R. (2018). Manipulating transmit and receive sensitivities of radiofrequency surface coils using shielded and unshielded high-permittivity materials. *Magnetic Resonance Materials in Physics, Biology and Medicine*, *31*(3), 355–366. https://doi.org/10.1007/s10334-017-0657-5

Varma, G., Girard, O. M., Mchinda, S., Prevost, V. H., Grant, A. K., Duhamel, G., & Alsop, D. C. (2018). Low duty-cycle pulsed irradiation reduces magnetization transfer and increases the inhomogeneous magnetization transfer effect. *Journal of Magnetic Resonance*, *296*, 60–71. https://doi.org/10.1016/j.jmr.2018.08.004

Vassiliou, V. S., Heng, E. L., Gatehouse, P. D., Donovan, J., Raphael, C. E., Giri, S., Babu-Narayan, S. V.,

Gatzoulis, M. A., Pennell, D. J., Prasad, S. K., & Firmin, D. N. (2016). Magnetic resonance imaging phantoms for quality-control of myocardial T1 and ECV mapping: Specific formulation, long-term stability and variation with heart rate and temperature. *Journal of Cardiovascular Magnetic Resonance*, *18*(1), 1–12. https://doi.org/10.1186/s12968-016-0275-9

Yongabi, D., Mertens, N., & Peeters, R. (2021). Reproducibility of T1 relaxation times in diagnostic MRI: A phantom study. *Physics in Medicine*, *12*. https://doi.org/10.1016/j.phmed.2021.100038

Yusuff, H., Chatelin, S., & Dillenseger, J.-P. (2024). Narrative review of tissue-mimicking materials for MRI phantoms: Composition, fabrication, and relaxation properties. *Radiography*, *30*(6), 1655–1668. https://doi.org/10.1016/j.radi.2024.09.063

Zhang, Q., Werys, K., Popescu, I. A., Biasiolli, L., Ntusi, N. A. B., Desai, M., Zimmerman, S. L., Shah, D. J., Autry, K., Kim, B., Kim, H. W., Jenista, E. R., Huber, S., White, J. A., McCann, G. P., Mohiddin, S. A., Boubertakh, R., Chiribiri, A., Newby, D., … Piechnik, S. K. (2021). Quality assurance of quantitative cardiac T1-mapping in multicenter clinical trials – A T1 phantom program from the hypertrophic cardiomyopathy registry (HCMR) study. *International Journal of Cardiology*, *330*, 251–258. https://doi.org/10.1016/j.ijcard.2021.01.026